

## **Ultrastable Radicals in Naphthalenediimide-Based Materials and their Stimulus-Boosting Near-Infrared Photothermal Conversion**

Hua Ke,<sup>a</sup> Xin-Mei Zhu,<sup>a</sup> Shu-Mei Xie,<sup>a</sup> Ping-Xiang Ming,<sup>a</sup> Jian-Zhen Liao<sup>ab\*</sup>

<sup>a</sup> Engineering Technology Research Center for Environmental Protection Materials, Pingxiang University, Pingxiang, Jiangxi 337055 (PR China); E-mail: [jjianzhenliao@sina.com](mailto:jjianzhenliao@sina.com)

<sup>b</sup> State Key Laboratory of Structural Chemistry, Fujian Institute of Research on the Structure of Matter, Chinese Academy of Sciences, Fuzhou, Fujian 350002 (PR China).

### **Table of Contents**

- 1. Materials and Physical Measurements**
- 2. Synthesis and Characterization**
- 3. Crystallographic Data Collection and Refinement**
- 4. Crystal Data for Complexes**
- 5. Related Figures**
- 6. References**

## 1. Materials and Physical Measurements

All chemicals were obtained from commercial sources and used as received without further purification. Powder X-ray diffraction (PXRD) analyses were performed on a Bruker D8 Advance diffractometer with Cu K $\alpha$  radiation ( $\lambda = 1.5418 \text{ \AA}$ ). Fourier transform infrared (FT-IR) spectra were collected in the range  $4000 - 400 \text{ cm}^{-1}$  on a PerkinElmer 2000 FT-IR spectrometer with pressed KBr pellets. Optical diffuse reflectance spectra were measured at room temperature on a Shimadzu UV-2600i UV-Vis-NIR spectrophotometer. Electron paramagnetic resonance (EPR) spectra were recorded on a Bruker BioSpin E500 EPR spectrometer with a 100 kHz magnetic field modulation at room temperature. Thermal analyses were performed on Netzsch STA 449F3 (TG-DSC) from room temperature to  $800^\circ\text{C}$  with a heating rate of  $10 \text{ K/min}$  under nitrogen. The fluorescence emission spectra were carried out by a FLS-1000 fluorescence spectrometer (Edinburgh Instruments).

## 2. Synthesis and Characterization

**Synthesis of N, N'-di(ethanesulfonic acid)-1,4,5,8-naphthalenediimide (denoted as H<sub>2</sub>TauNDI).** The ligand was synthesized according to the procedure in reference.<sup>[S1]</sup> A mixture of 1,4,5,8-naphthalene-tetracarboxylic dianhydride (NDA) (1.41 g, 5.26 mmol) and taurine (1.316 g, 10.52 mmol) in DMF (25 mL) was heated under 423 K for about 19 h. When the reaction mixture reached room temperature, NDI ligands were precipitated out, which was collected by filtration.

**Synthesis of complex Rb-NDI.** A mixture of H<sub>2</sub>TauNDI ligand (0.0482 g, 0.1 mmol), Rb<sub>2</sub>CO<sub>3</sub> (0.0231 g, 0.1 mmol), EtOH (1 mL) and dilute nitric acid (3 mL) were heated in a 20 mL brown Vial at  $95^\circ\text{C}$  for 3 days, followed by programmed cooled for 1 day to room temperature. Herein, the dilute nitric acid was the solution of 0.5 mL concentrated nitric acid (the concentrated nitric acid was commercially available, the labeled concentration was 65% - 68%.) dissolved in 200 mL water. After suction filtration, the brown crystals were collected. Yield: 59% (based on Rb). FT-IR ( $\text{cm}^{-1}$ ): 3446 (m), 1707 (m), 1659 (s), 1450 (m), 1383 (m), 1346 (s), 1256 (s), 1202 (s), 1050 (s), 880 (w), 804 (m), 769 (m).

**Synthesis of complex Cs-NDI.** A mixture of H<sub>2</sub>TauNDI ligand (0.0482 g, 0.1 mmol), Cs<sub>2</sub>CO<sub>3</sub> (0.00325 g, 0.1 mmol), EtOH (1 mL) and dilute nitric acid (3 mL) were heated in a 20 mL brown

Vial at 95°C for 3 days, followed by programmed cooled for 1 day to room temperature. Herein, the dilute nitric acid was the solution of 0.5 mL concentrated nitric acid (the concentrated nitric acid was commercially available, the labeled concentration was 65% - 68%.) dissolved in 200 mL water. After suction filtration, the deep yellow crystals were collected. Yield: 50% (based on Cs). FT-IR ( $\text{cm}^{-1}$ ): 3444 (m), 1707 (m), 1659 (s), 1457 (s), 1387 (m), 1350 (m), 1263 (s), 1200 (s), 1102 (w), 1040 (s), 880 (w), 804 (m), 763 (m).

**Photothermal conversion properties measurement.** The 50 mg **Rb-NDI** (or **Cs-NDI**) original sample, irradiated sample (after irradiated by blue light for 10 min) and that after heating treatment sample (after heating treatment at 300 °C for 3h) were pressed into 5-mm-diameter pellets using a manual tablet press at the pressure of 3.75 Mpa, respectively. The obtained pellets was under continuous irradiation of a 808 nm laser until the sample reached a steady-state temperature. The temperature was monitored every 10 s by a Fluke (Ti400+) thermal imaging camera. The 808 nm laser beam was irradiated at a power density from 0.4 to 2.5  $\text{W cm}^{-2}$ .

**Solid state cyclic voltammetry.** Cyclic voltammetry (CV) studies of **Rb-NDI** and **Cs-NDI** were carried out using a computer controlled potentiostat (CHI 760E) and a standard three electrode arrangement that consisted of both platinum working and auxiliary electrodes and Ag/AgCl as reference electrode. The working electrode should be ground with  $\text{Al}_2\text{O}_3$  powder before use. All CV curves were measured in DMF under a nitrogen atmosphere at room temperature and a scanning rate of 100 mV/s using  $\text{n-Bu}_4\text{NPF}_6$  (0.1 M) as a supporting electrolyte. Ferrocene (Fc, 5 mM) was used as a standard for calibration. The microcrystalline **Rb-NDI** (or **Cs-NDI**) complex was coated onto the surface of the working electrode by dipping the electrode in a slurry of the solid with acetone.

### 3. Crystallographic Data Collection and Refinement

A suitable crystal of complexes **Rb-NDI** or **Cs-NDI** was selected and collected on a XtaLAB Synergy R, HyPix diffractometer. Using Olex2<sup>[S2]</sup>, the structure was solved with the ShelXS<sup>[S3]</sup> structure solution program using Direct Methods and refined with the ShelXL<sup>[S4]</sup> refinement package using Least Squares minimisation. Crystallographic data has been deposited at the Cambridge Crystallographic Data Center with reference number CCDC 2152350 and 2152351.

These data can be obtained free of charge from The Cambridge Crystallographic Data Centre via [http://www.ccdc.cam.ac.uk/data\\_request/cif](http://www.ccdc.cam.ac.uk/data_request/cif).

#### 4. Crystal Data for Rb-NDI and Cs-NDI

**Crystal Data for complex Rb-NDI** ( $\text{C}_9\text{H}_6\text{NO}_5\text{RbS}$ ,  $M_r = 325.68$  g/mol): monoclinic, space group  $P2_1/c$  (no. 14),  $a = 17.6426(2)$  Å,  $b = 7.63130(10)$  Å,  $c = 7.86490(10)$  Å,  $\beta = 96.0960(10)^\circ$ ,  $V = 1052.91(2)$  Å<sup>3</sup>,  $Z = 4$ ,  $T = 293(2)$  K,  $\mu(\text{CuK}\alpha) = 8.463$  mm<sup>-1</sup>,  $D_{\text{calc}} = 2.054$  g/cm<sup>3</sup>, 16362 reflections measured ( $5.038^\circ \leq 2\theta \leq 150.824^\circ$ ), 2114 unique ( $R_{\text{int}} = 0.0224$ ,  $R_{\text{sigma}} = 0.0111$ ) which were used in all calculations. The final  $R_1$  was 0.0368 ( $I > 2\sigma(I)$ ) and  $wR_2$  was 0.0985 (all data).

**Crystal Data for complex Cs-NDI** ( $\text{C}_9\text{H}_6\text{CsNO}_5\text{S}$ ,  $M_r = 373.12$  g/mol): orthorhombic, space group  $Pbca$  (no. 61),  $a = 7.82263(5)$  Å,  $b = 7.97884(5)$  Å,  $c = 35.6040(2)$  Å,  $V = 2222.24(2)$  Å<sup>3</sup>,  $Z = 8$ ,  $T = 293(2)$  K,  $\mu(\text{CuK}\alpha) = 27.891$  mm<sup>-1</sup>,  $D_{\text{calc}} = 2.230$  g/cm<sup>3</sup>, 62885 reflections measured ( $4.964^\circ \leq 2\theta \leq 150.814^\circ$ ), 2280 unique ( $R_{\text{int}} = 0.0846$ ,  $R_{\text{sigma}} = 0.0189$ ) which were used in all calculations. The final  $R_1$  was 0.0288 ( $I > 2\sigma(I)$ ) and  $wR_2$  was 0.0771 (all data).

#### 5. Related Figures

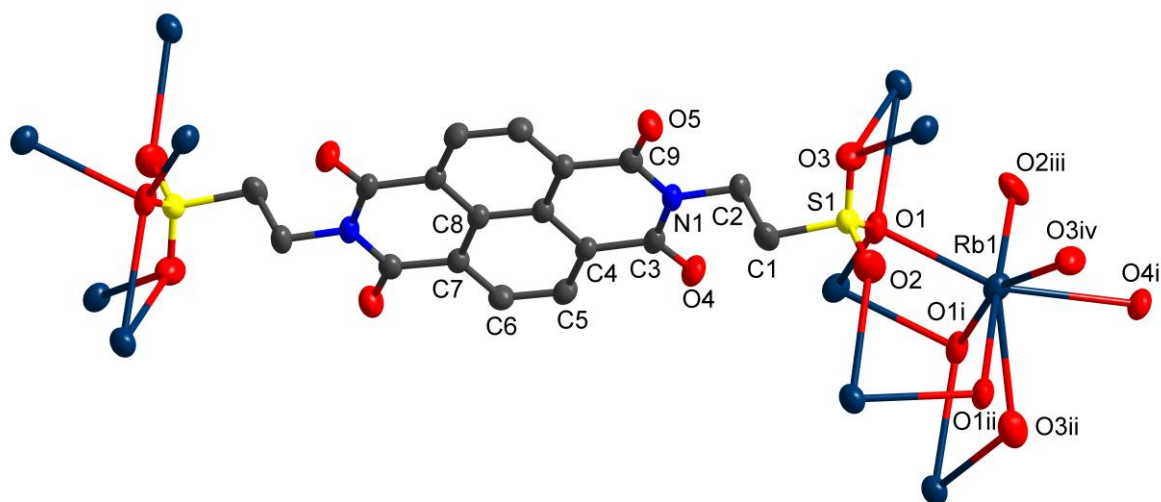


**Figure S1.** Coordination environment of the Rb(I) cations in **Rb-NDI**. Symmetry codes: i)  $1-x, 1-y, 1-z$ ; ii)  $1-x, 0.5+y, 0.5-z$ ; iii)  $1-x, -0.5+y, 0.5-z$ ; iv)  $1-x, 1-y, -z$ .

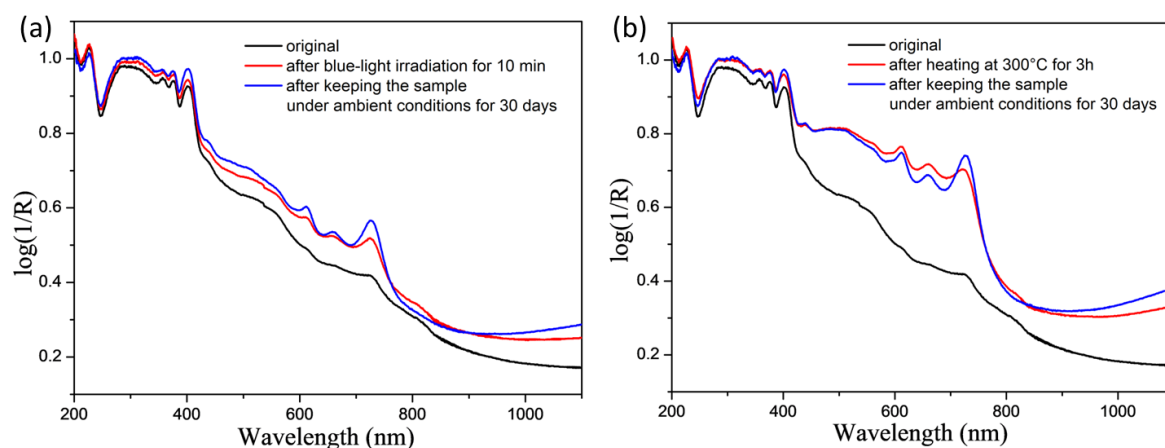


**Figure S2.** a) The changes for the UV-Vis NIR absorption spectra of the blue-light irradiated **Rb-NDI** sample after placed in air for one month; b) The changes for the UV-Vis NIR absorption spectra of the thermal-activated **Rb-NDI** sample after placed in air for one month.

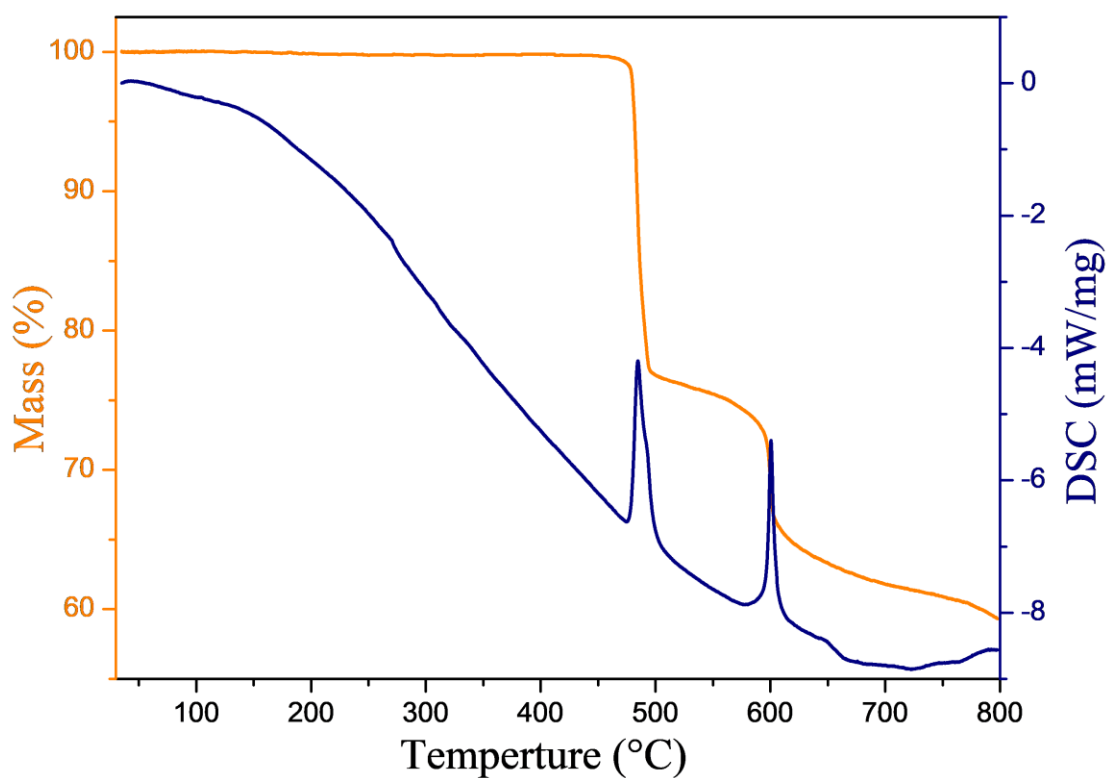


**Figure S3.** The TGA/DSC curves for **Rb-NDI**.

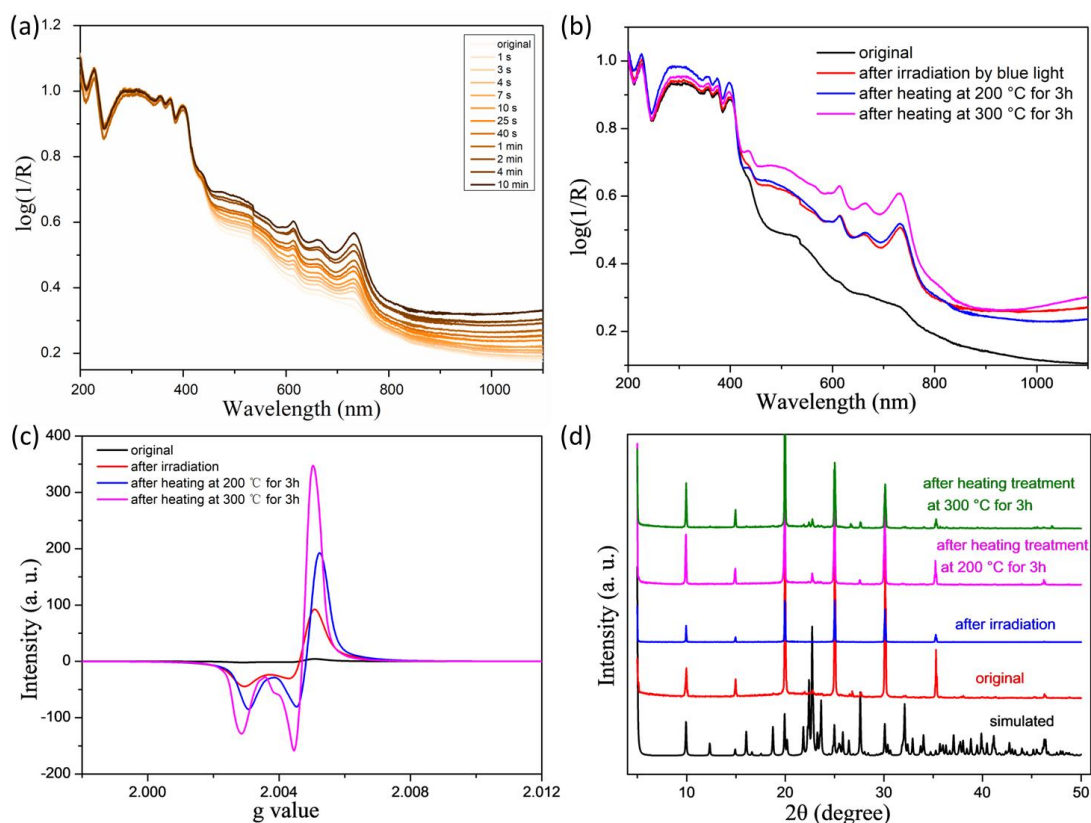


**Figure S4.** (a) *In-situ* solid state UV-Vis-NIR spectra for **Cs-NDI** with different irradiation time; (b) Solid state UV-Vis-NIR spectra for **Cs-NDI** under different treatments; (c) The EPR spectra of **Cs-NDI** under different treatments; (d) PXRD patterns of **Cs-NDI** under different treatments.

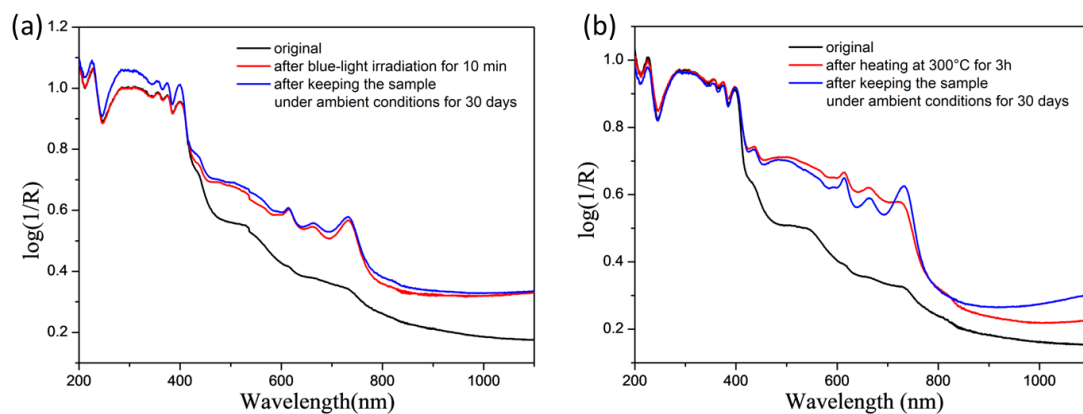


**Figure S5.** a) The changes for the UV-Vis NIR absorption spectra of the blue-light irradiated **Cs-NDI** sample after placed in air for one month; b) The changes for the UV-Vis NIR absorption spectra of the thermal-activated **Cs-NDI** sample after placed in air for one month.

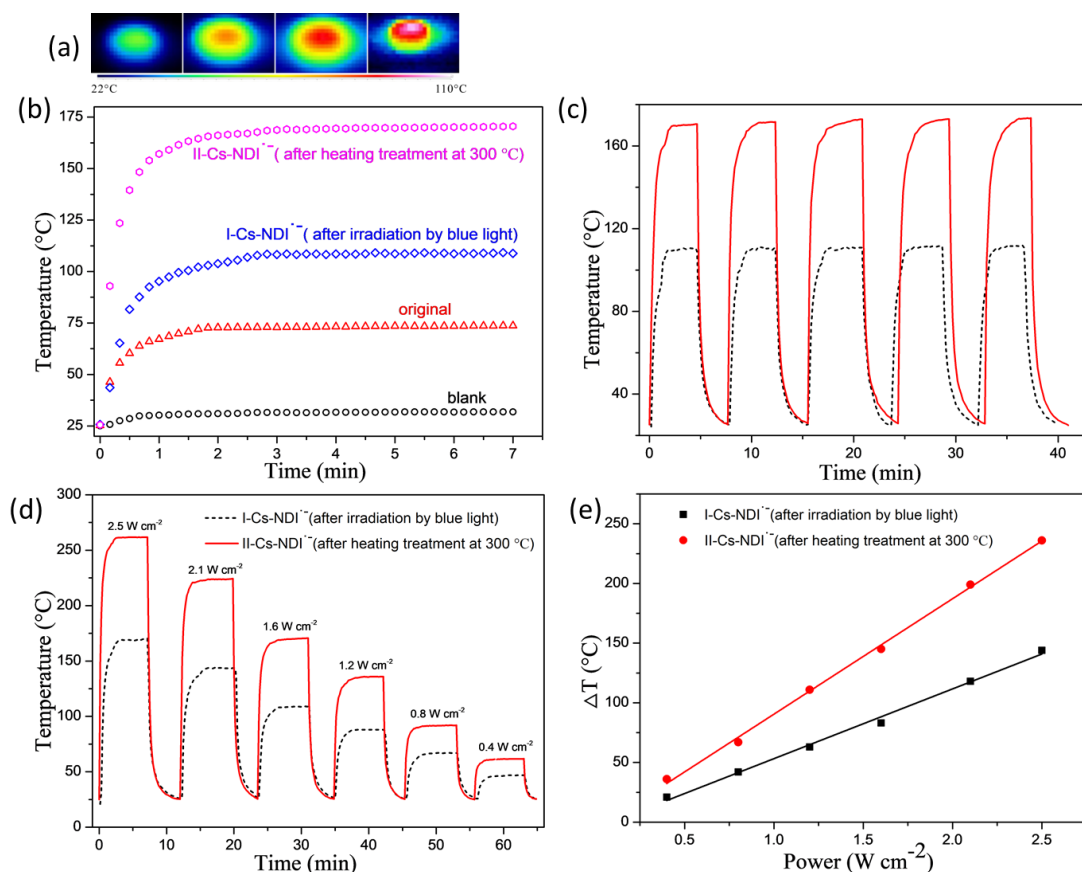


**Figure S6.** (a) Infrared thermal images of **Cs-NDI** solid sample; (b) The controlled experiments for photothermal conversion of **Rb-NDI** sample under 808 nm laser irradiation (1.6 W cm<sup>-2</sup>); (c) Photothermal conversion cycling curve for **Cs-NDI** solid sample under 808 nm laser irradiation (1.6 W cm<sup>-2</sup>); (d) Temperature changes for **Cs-NDI** under different NIR laser intensities; (e) The function between the average temperature rise and NIR laser intensities.

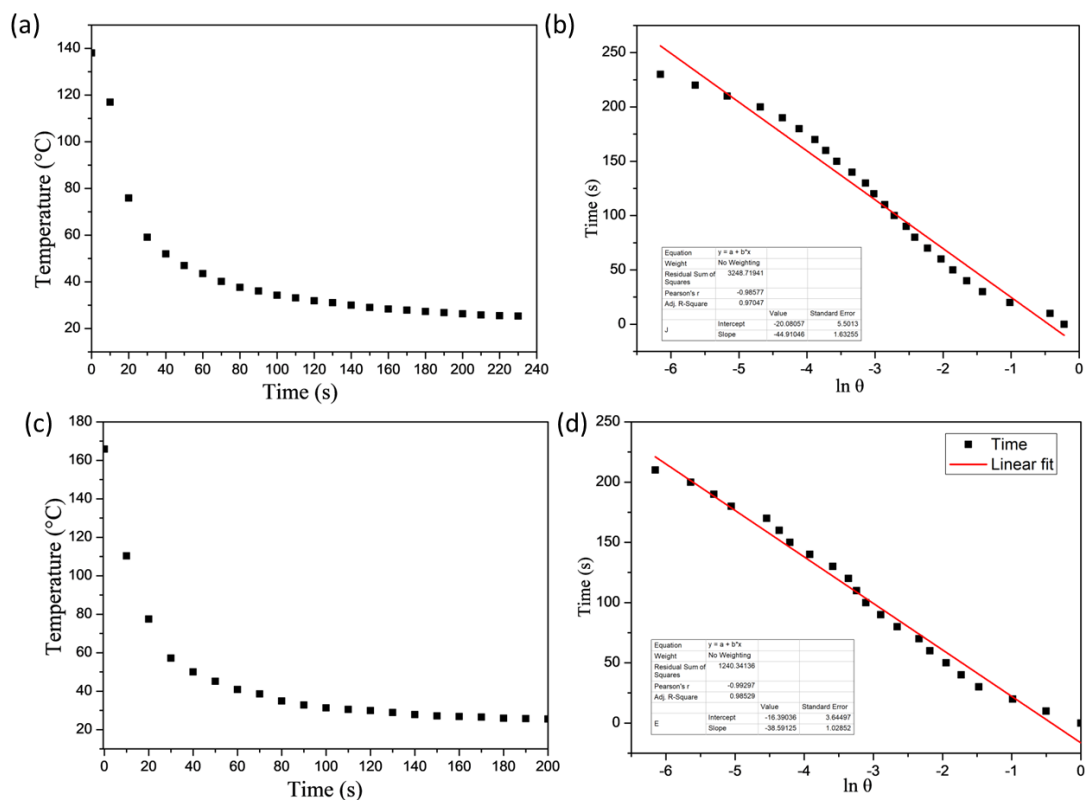


**Figure S7.** (a) The cooling curve of **I-Rb-NDI** film after irradiation with 808 nm laser ( $1.6 \text{ W cm}^{-2}$ ); and its corresponding time- $\ln\theta$  linear curve (b); (c) The cooling curve of **II-Rb-NDI** film after irradiation with 808 nm laser ( $1.6 \text{ W cm}^{-2}$ ) and its corresponding time- $\ln\theta$  linear curve (d).



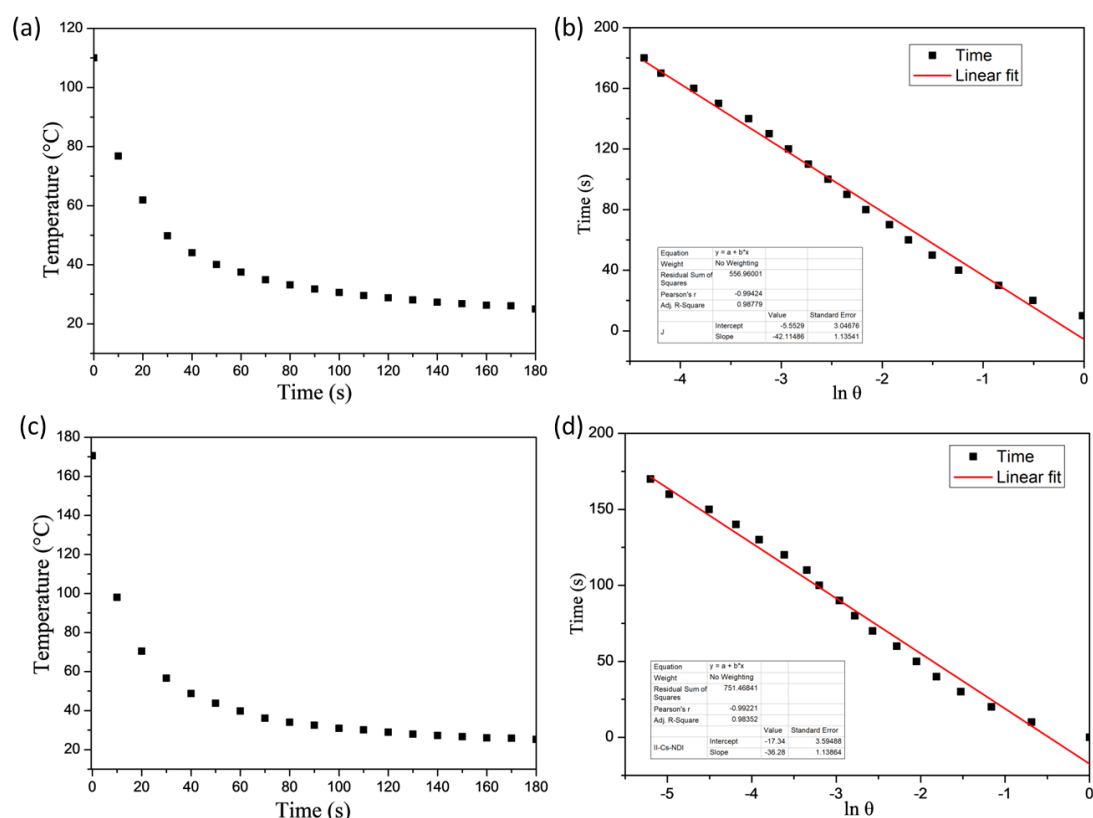


**Figure S8.** (a) The cooling curve of **I-Cs-NDI** film after irradiation with 808 nm laser ( $1.6 \text{ W cm}^{-2}$ ) and its corresponding time- $\ln\theta$  linear curve (b); (c) The cooling curve of **II-Cs-NDI** film after irradiation with 808 nm laser ( $1.6 \text{ W cm}^{-2}$ ) and its corresponding time- $\ln\theta$  linear curve (d).

**Table S1** Experimental values of  $\log(1/R)$ ,  $\Delta T_{\max}$ ,  $\tau_s$ , and  $\eta$  calculated from UV-Vis-NIR spectra and photothermal conversion test for compounds under different treatments.

Compound	$\log(1/R)(\text{a.u.})$	$\Delta T_{\max}(\text{°C})$	$\tau_s$ (the slope of cooling time vs $\ln \vartheta$ )	$\eta$
<b>I-Rb-NDI</b>	0.342	113	44.9	23.3%
<b>II-Rb-NDI</b>	0.374	141	38.6	32.1%
<b>I-Cs-NDI</b>	0.289	86	42.1	31.5%
<b>II-Cs-NDI</b>	0.365	145	36.3	52.6%

The conversion efficiency was determined according to previous method.<sup>S6-S8</sup>

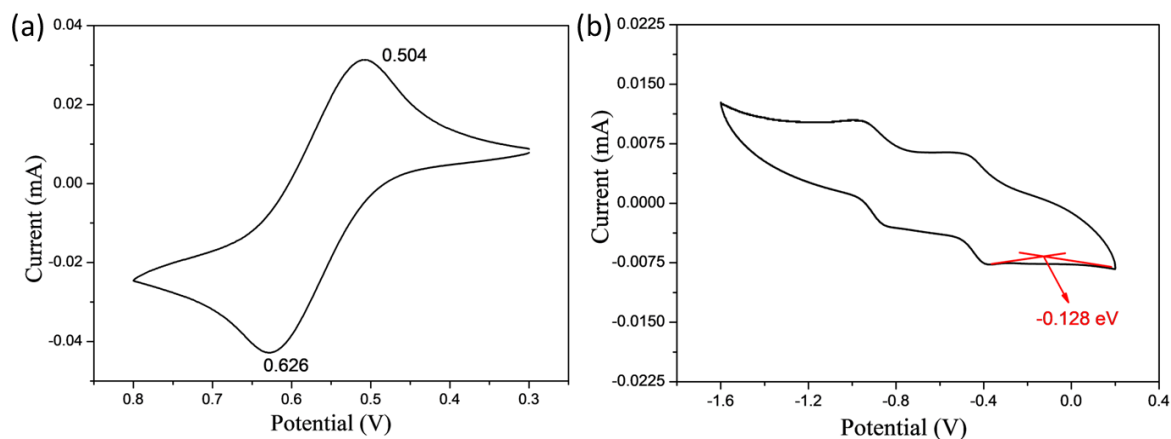


**Figure S9.** a) CV of Fc in 0.1 M n-Bu<sub>4</sub>NPF<sub>6</sub>/DMF at a scanning rate of 100 mV/s; b) Solid-state CV of Cs-NDI in 0.1 M n-Bu<sub>4</sub>NPF<sub>6</sub>/DMF at a scanning rate of 100 mV/s.

**Table S2** Experimental values of onset reduction potential ( $E_{\text{red}}$ ); experimental values of optical bandgap,  $E_{\text{LUMO}}$ , and  $E_{\text{HOMO}}$  calculated from UV-Vis spectra and CVs.

Compound	$E_{\text{red}}^a$ (V)	$E_{\text{LUMO}}^b$ [eV]	Optical bandgap [eV]	$E_{\text{HOMO}}^c$ [eV]
<b>Rb-NDI</b>	-0.22	-4.02	2.11	-6.13
<b>Cs-NDI</b>	-0.13	-4.11	2.43	-6.54

a)  $E_{\text{red}}$  was obtained from CV diagrams<sup>S5</sup>; b)  $E_{\text{LUMO}} = -(E_{\text{red}} + 4.80 - E_{1/2, \text{Fc}})^{\text{S5}}$ ; c)  $E_{\text{HOMO}} = E_{\text{LUMO}} + \text{Optical bandgap}^{\text{S5}}$

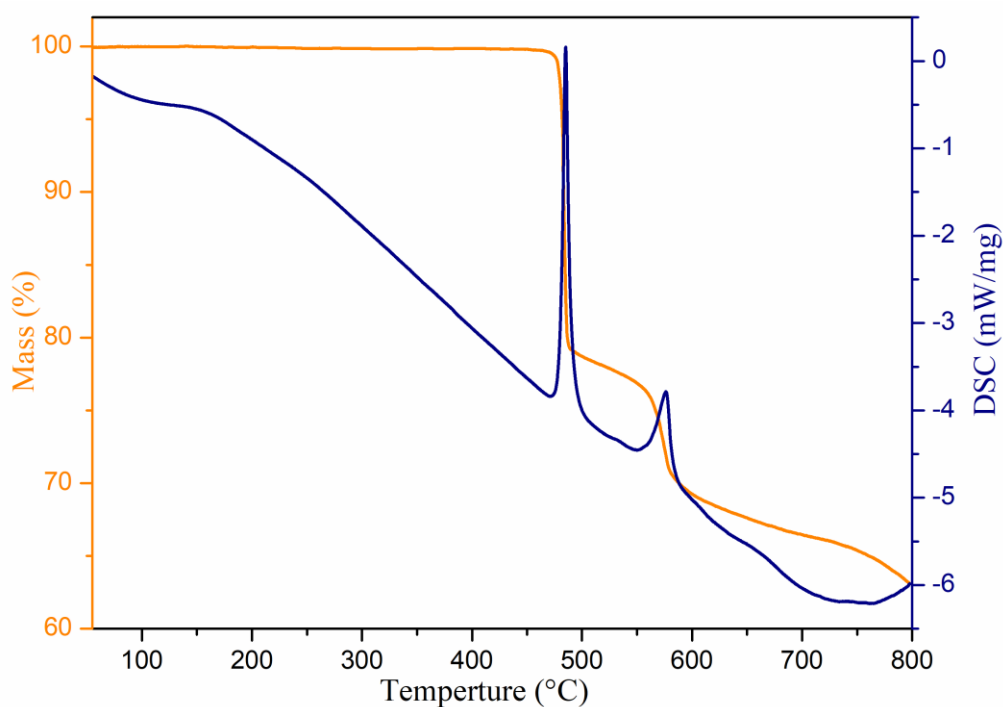


**Figure S10.** The TGA/DSC curves for **Cs-NDI**.

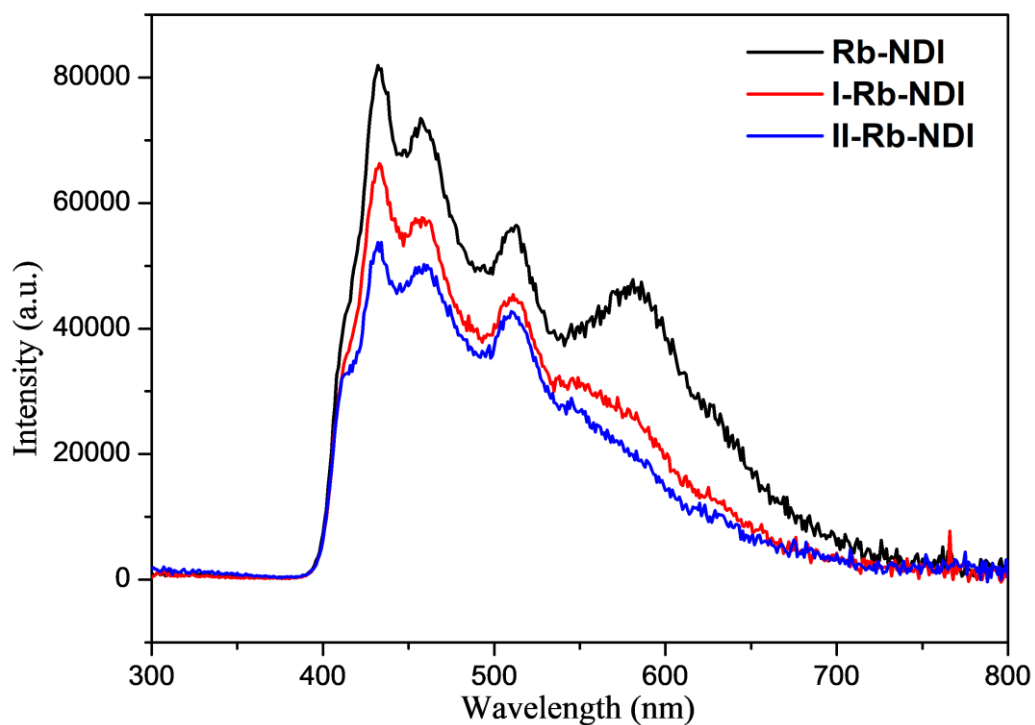


**Figure S11.** The fluorescence emission spectra ( $\lambda_{\text{ex}} = 280 \text{ nm}$ ) for **Rb-NDI** before and after irradiation by LED blue-light ( $\lambda = 460 - 465 \text{ nm}$ ) for 10 min, and the sample after heating at  $300^\circ\text{C}$  for 3 h.

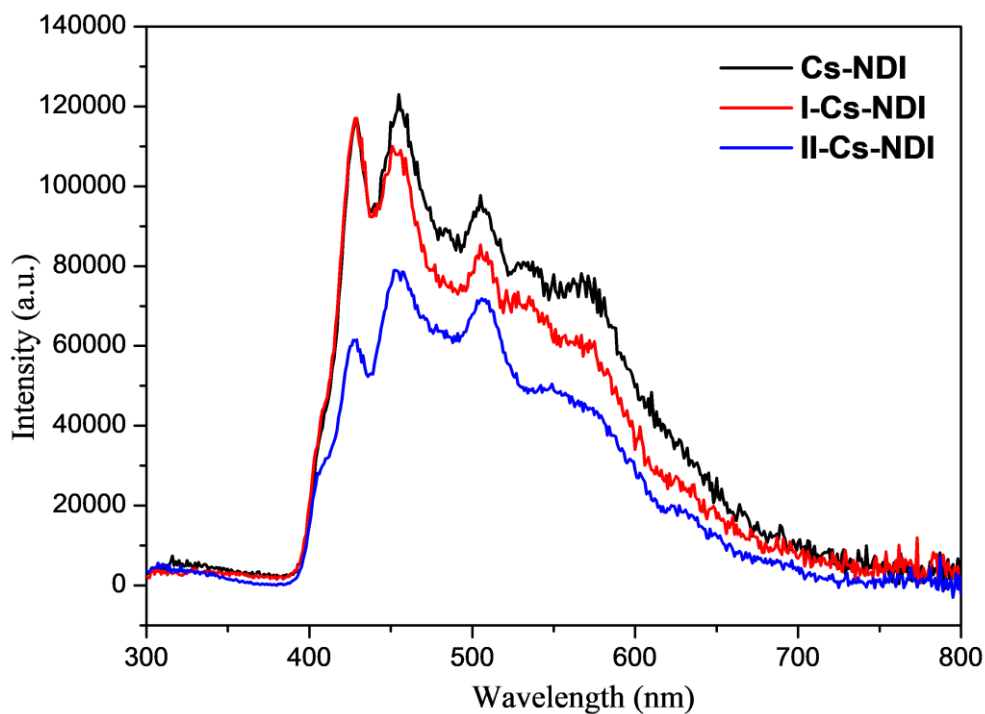


**Figure S12.** The fluorescence emission spectra ( $\lambda_{\text{ex}} = 280 \text{ nm}$ ) for **Cs-NDI** before and after irradiation by LED blue-light ( $\lambda = 460 - 465 \text{ nm}$ ) for 10 min, and the sample after heating at  $300^\circ\text{C}$  for 3 h.

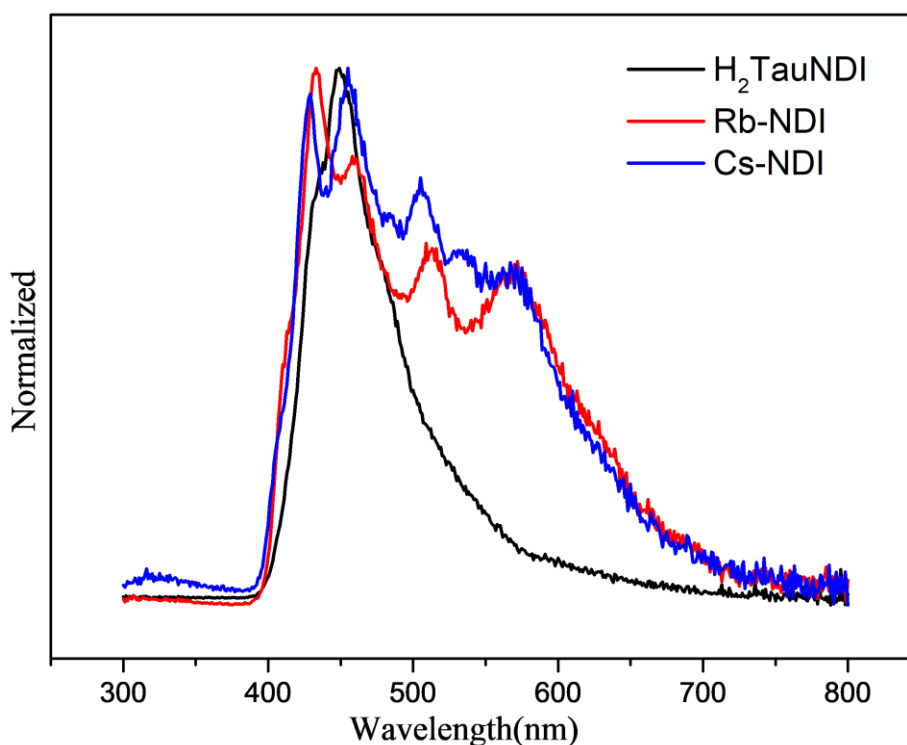


**Figure S13.** The emission spectra for the H<sub>2</sub>TauNDI ligand ( $\lambda_{\text{ex}} = 300$  nm), **Rb-NDI** ( $\lambda_{\text{ex}} = 280$  nm) and **Cs-NDI** ( $\lambda_{\text{ex}} = 280$  nm) in the solid state.

Their fluorescence spectra are shown in above figure S11-S13, demonstrating that if the materials possess more organic radicals will be with a weaker light emission, in agreement with a higher photothermal conversion.

## 6. Reference

- S1 J. Z. Liao, J. F. Chang, L. Meng, H. L. Zhang, S. S. Wang, C. Z. Lu, *Chem. Commun.* **2017**, 53, 9701.
- S2 Dolomanov, O.V., Bourhis, L.J., Gildea, R.J., Howard, J.A.K. Puschmann H. *J. Appl. Cryst.*, 2009, **42**, 339.
- S3 Bourhis, L.J., Dolomanov, O.V., Gildea, R.J., Howard, J.A.K., Puschmann, H. *Acta Cryst.*, 2015, *A71*, 59.
- S4 Sheldrick, G.M. *Acta Cryst.*, 2015, **C71**, 3.
- S5 Li F, Huang Z, Zhou Q, Pan M, Tang Q, Gong C. *J. Mater. Chem. C*, 2020, **8**, 10031.
- S6 Kim B, Shin H, Park T, Lim H, Kim E. *Adv. Mater.*, 2013, **25**, 5483.
- S7 Lü B, Chen Y, Li P, Wang B, Müllen K, Yin M. *Nat. Commun.*, 2019, **10**, 767.
- S8 Li M.-Q, Zhao M, Bi L.-Y, Hu Y.-Q, Gou G, Li J, Zheng Y.-Z. *Inorg. Chem.*, 2019, **58**, 6601.